


RESEARCH

Open Access



Characterising fragmentation of compostable bioplastic: releasing microplastics or small bioplastic debris

Cheng Fang^{1,2*} , Xian Zhang³, Zixing Zhang³ and Ravi Naidu^{1,2}

Abstract

Background Plastic is generating global pollution and the replacement such as bioplastic has been developed to mitigate the pollution. To this end, the fate, transformation and pathway of bioplastics need more research. For example, the fragmentation of bioplastic can release small debris that can be categorised as microplastics, which is tested herein by taking an example of a compostable plastic that is used as a bin bag on our kitchen table to collect the food residues.

Results First, we employ matrix-assisted laser desorption/ionisation mass spectrometry (MALDI-MS) to identify the main components of the bioplastic bag as polymer and starch. Next, we use Raman imaging to monitor the stability under laser illumination, in an oven at ~60 °C for ~2 weeks, or in the presence of tap water for half a year. Basically, the compostable plastic is stable under these conditions. Thirdly, however, once used as table-bin bag with involvement of food residues, within ~1 week, the bioplastic bag is broken and biodegraded to release debris. The derivate surface groups are effectively monitored and directly visualised via Raman imaging, and cross-checked with scanning electron microscope (SEM). The yielded small molecule such as formic acid is also identified, along with the released debris of microplastics, with the help of on-site extraction of the fragmented sample and imaging analysis algorithm of the hyper spectrum.

Conclusions After one week, the bag in the waste bin fragments, releasing a significant amount of debris. This could pose a functional issue if users intend to use the bag for at least a week, and could become a potential environmental problem if the waste is dispersed uncontrollably. In general, further research is needed to potentially distinguish the persistent conventional microplastics from the bioplastic fragments, to effectively mitigate the plastic pollution.

Keywords Bioplastic, Compostable plastic, Raman imaging, Fragmentation, Microplastic, Derivation surface group

*Correspondence:

Cheng Fang

cheng.fang@newcastle.edu.au

Full list of author information is available at the end of the article



© The Author(s) 2024. **Open Access** This article is licensed under a Creative Commons Attribution 4.0 International License, which permits use, sharing, adaptation, distribution and reproduction in any medium or format, as long as you give appropriate credit to the original author(s) and the source, provide a link to the Creative Commons licence, and indicate if changes were made. The images or other third party material in this article are included in the article's Creative Commons licence, unless indicated otherwise in a credit line to the material. If material is not included in the article's Creative Commons licence and your intended use is not permitted by statutory regulation or exceeds the permitted use, you will need to obtain permission directly from the copyright holder. To view a copy of this licence, visit <http://creativecommons.org/licenses/by/4.0/>.

Graphical Abstract



Introduction

The increasing concern on plastic pollution leads to the exploration on replacement, such as bioplastics that are intentionally designed to be environmentally friendly and sustainable [1]. As the replacement to conventional plastics that are derived from fossil fuels, bioplastics are typically made from biobased or biodegradable materials (or features both properties). While some conventional plastics are also biodegradable, biobased plastics are partially or totally formulated with plant-based/derived materials such as corn starch, microorganisms, or renewable / recycled materials [2, 3]. Generally, bioplastics particularly biobased plastics have some benefits such as reduced carbon footprint and dependency on the fossil fuels, but also face with some challenges including cost (more expensive than the conventional plastics) and performance (may not have the same physical properties / durability as the conventional plastics). Like the conventional plastics, the bioplastics might also contaminate the environment if not properly treated, so that different countries have different regulations on bioplastics [1]. For example, for compostable plastics, ideally via biodegradation in a composting environment, they should break down into water and carbon dioxide with help of microorganisms within a reasonable timeframe (according to industrial composting standards such as EN 13432, ASTM D6400, ISO 17088, EN 14995). If not completely broken down during the pathway, the biodegradation or fragmentation might still release some debris. Those bioplastic fragments or debris can also be categorised as microplastics (< 5 mm), which is studied herein [4–6].

Plastic pollution refers to the accumulation of non-degradable plastic waste in the environment including oceans, rivers, forests, and urban areas [7]. When the plastic wastes are large (> 5 mm) to be seen by our naked eyes, concern arises particularly from publics. Consequently, with the recent advancements, these large plastics can be reused, recycled or re-produced to harvest energy [1]. However, the small plastics or microplastics that cannot be directly seen by our naked eyes might be more serious in terms of environmental pollution or contamination [8]. Microplastics can either result from the breakdown of large plastics due to weathering, UV radiation, and physical abrasion, or are intentionally manufactured at a small size for various applications [9–11]. They are difficult to be recycled, and as emerging contaminant, we do not yet know too much about them including their source, fate, toxicity, etc. Regarding their source, for example, various domestic plastic items in our daily lives can release debris as microplastics even nanoplastics (< 1000 nm), for which we do not yet pay enough attention [12, 13]. As a replacement of the conventional plastic, bioplastics might also work as the similar sources of microplastics and nanoplastics in our daily lives, which is main objective of this report [1, 4, 5].

Unfortunately, not matter for the conventional plastics or the bioplastics, the analysis on microplastics is difficult due to the shrink size, complex ingredient, environmental background, abundant plastic types, etc. [9, 10, 12–16]. So far, the available analysis approaches for microplastics include microscopy (optical, scanning electron microscope or SEM, transmission electron microscope or TEM, atomic force microscope or AFM),

atomic analysis (energy-dispersive X-ray spectroscopy or EDS, X-ray photoelectron spectroscopy or XPS, thermogravimetric analysis or TGA), mass spectrum (pyrolysis gas chromatography mass spectrometry or py-GC-MS, matrix-assisted laser desorption/ionisation mass spectrometry or MALDI-MS) and molecular spectrum (fluorescence, UV-vis, Raman and infrared or IR). They can effectively analyse microplastics, but all have the limitations. Microscopy and atomic analysis can provide the morphological and element composition information, respectively, but they cannot identify plastics. Mass and molecular spectra can identify plastics, but without the morphological information for visualisation and quantification of microplastics. To overcome those challenges, either they can be combined to benefit each other (such as SEM + Raman) [17], or mass / molecular spectrum is advanced and mapped to generate image (imaging analysis) towards visualisation and quantification [12, 13].

Among the imaging analysis, Raman imaging is a technique to combine Raman spectrometer with a microscopy as micro-Raman [14]. By scanning an excitation laser with help of microscopy, Raman spectrometer can collect spectrum at the specific positions (pixels), gradually as a spectrum array, or hyper spectrum or a hyper-spectral matrix. From this hyper spectrum that can contain hundred-to-thousand spectra (depending on the scan parameters or resolution), each spectrum is mapped at the spectrum-collection position as a pixel. Consequently, the mapping can generate a spectrum image that provides the morphological information from the molecular spectrum window, a main advantage. Other advantages include the high mapping resolution (using short wavelength of laser, not IR), non-damage analysis, no interference from water, easy interpretation of spectrum, etc. The accompanied challenge is, the hyper spectrum is of big dataset at size of MB or even GB. This “big data” analysis needs help of algorithm, such as chemometrics. Other challenges include the time-consuming process (scanning), expensive setup and resolution limitation originating from the laser diffraction [14, 18, 19]. Furthermore, the Raman spectrum interpretation of the coloured, aged, environmental and biological samples are also difficult due to the strong background interference.

In this report, we test the stability of a typical compostable plastic, which is generally used in our kitchen as a table-bin bag, distributed by a local council in Australia in effort to reduce home-made rubbish and mitigate the plastic pollution. We first employ MALDI-MS to identify the main components in the bioplastic. The fragmentation of the compostable plastic in kitchen is then monitored by Raman imaging, to confirm the released small debris as microplastics or bioplastic fragments. That is, during a not-well-controlled fragmentation process (not

via an industrial composting facility), the compostable plastic can release microplastics. As the first research in this field, lots of unknowns are still open and the results herein are helpful for future research, such as to compare the released bioplastic fragments with the conventional microplastics, in terms of fate, pathway, toxicity and risk assessment.

Materials and methods

Chemicals and samples

All chemicals including ethanol and virgin plastic of polyethylene terephthalate (PET) were purchased from Sigma-Aldrich (Australia) and used as received. Pure water (> 18 M Ω cm, or Milli Q water) was used for the analysis. Bioplastics bags are purchased from local markets (Woolworths, Coles, ALDI, Australia) or collected from a local council (Lake Macquarie, NSW, Australia) in 2023, as shown in Figures S1-S2/Table S1 (Supporting information). We tested several typical ones including a compostable bag (#1), a plant-based bag (#2), a sustainable bag (#3), a garbage bag (#4), a compostable earth-friendly bag (#5) and an ocean plastic-recycled bag (#6). Herein the bag #1 of bioplastic was focused, which has been used as a bin bag on the kitchen table in Australia to collect the food residues. Another one (#7) for the similar application in China was also tested in parallel to increase the representativeness.

For stability test shown in Figures S3-S5 (Supporting Information), the bags were cut to small size using a stainless scissors. The marking areas with logo or brand information were intentionally avoided. They were then cleaned with ethanol, acetone and Milli Q water. The samples were fixed onto the glass slide surface with paper mask, as shown in Figure S6 (Supporting Information). These samples can be directly tested to check the stability under the laser illumination, and to collect the Raman spectra as the “mother” spectra of the plastic samples.

The above samples were incubated in an oven at ~ 60 °C in air for ~ 2 weeks first. During this period, the samples were tested daily, to monitor the change of the Raman spectrum. After that, the samples were localised onto an aluminium island surrounded by tap water in a glass container, as shown in Figure S6 (Supporting Information). The container was not completely sealed and kept at ~ 38 °C, for half a year. During this period, the samples were tested monthly.

Different from above samples, we also collected samples from the kitchen table-bin bag, also presented in Figure S6 (Supporting Information). The bag has been used for ~ 1 week (the bin collection period by the local council. For a shorter time such as within 3 days, no obvious degradation was observed), in the early summer (September 2023) in Newcastle, NSW, Australia, to collect

the food residues. The food residues included onion skin, carrot skin, banana skin, avocado skin, ginger skin, kiwi skin, chinese cabbage, etc. The bag was degraded and broken. We padded the bag, under the bag we employed several printing papers (A4) to collect the debris. The slight-green can help to identify the bag debris while food residues were removed using a stainless tweezer. The collected debris were tested within one week.

Before testing, the collected samples were washed with Milli Q water and ethanol. The washing with Milli Q water was last for ~5 min and with ethanol for another ~5 min to clean the surface. The washing process can be prolonged to ~3 days in order to completely clean the surface, as indicated below. The samples were then transferred onto glass slide for test, as shown in Figure S7 (Supporting Information). On the glass slide surface in the meantime, we can also conduct on-site extraction, by dropping a droplet of ethanol (~10 μ L) on the sample surface, after evaporation and dried, another droplet was added and repeated for 5 times. The evaporation of ethanol can lead to the capillary force to help the extraction of small particles / fragments (1–25 μ m) from the big ones (> 100 μ m) [20].

After Raman test, the glass slide was cut using a strong stainless scissors to small pieces (~2 cm \times ~2 cm) for SEM test. During this cutting process, the big pieces might fly away from the glass surface, leading to the difference between the Raman image and the SEM image. For SEM test, a thin layer of palatium (~10 nm) was sputter-coated on the surface to increase the conductivity.

MALDI-MS

Similarly, bioplastic table-bin bags were cut by scissors to small pieces (<1 mm) and solved in an acetonitrile solution (~0.1 g in ~1 mL). Then the solution of ~2 μ L was deposited on a matrix surface of indium tin oxide (ITO). After drying in air, a solution of 2,5-dihydroxybenzoic acid (~20 mg/mL) in acetonitrile—0.1% trifluoro acetic acid (30:70, v/v) was sprayed on the droplet surface [21]. After drying, the sample was placed in an instrument for MALDI mass spectra analysis, which was acquired on the UltrafleXtreme MALDI-TOF/TOF MS system (Bruker Daltonic Inc., USA). The MS acquisition parameters were briefed as follows: ion polarity, positive; mass range, 600–3500; sample voltage, 3.50 kV; detector voltage, 1.80 kV. Laser firing parameters were pitch (20 μ m), repetition rate (1000 Hz) and intensity (30).

Raman testing protocols and data analysis algorithms

The testing protocols were reported before [22, 23]. In brief, Raman spectra were recorded using a confocal Raman microscope (DXRxi / ThermoFisher, USA) equipped with 532 nm or 785 nm laser diode (~30

mW), charge-coupled device (CCD) detector (cooled at -60 $^{\circ}$ C) to collect Stokes Raman signals, under an objective lens (100 \times , or others such as 50 \times , 20 \times and 10 \times) and at the room temperature (~24 $^{\circ}$ C). We first used the maximum laser power to check the potential damage to the sample by laser burning, as stated below. However, after the fragmentation, we must decrease the laser power to minimum to avoid the laser burning.

To map the image, the laser was scanning on the sample surface to collect the signal at each pixel or point. The signal intensity at the selected peak can be mapped as RGB (red, green, blue) to visualise the distribution. The scanning array (such as 30 \times 30) was controlled by adjusting the pixel size (such as 30 μ m \times 30 μ m, which can be defined as image resolution) and the scan area (such as 900 μ m \times 900 μ m). By doing so, we can also realise the zooming-in scanning by shrinking the pixel size and scan area. To map image, the spectrum background was intentionally removed by subtracting the baseline at the two sides of the selected peak.

There are many peaks in a spectrum, each peak can generate an image. These images can be cross-checked and merge to compare them in the same image. To this end, ImageJ software was employed and the colour-channel-merge function was used. The mapped Raman image can also be overlapped onto the photo image or the SEM image as well, using the similar approach.

The whole set of spectrum (not just the selected peak) can be mapped to generate image as well. In this case, chemometrics is needed, such as via correlation calculation to compare the sample spectrum with a reference spectrum, or a standard spectrum of the suspected item. To this end, we normalise the sample spectrum and the reference spectrum intensities to 0–1 (such as using function " $(x_i - x_{min}) / (x_{max} - x_{min})$ "). We then calculate the correlation value at each pixel to map an image. The software of OMNICxi for the DXRxi Raman can realise this function.

Particle analysis

For particle analysis, ImageJ software was employed again [24]. In brief, after an image was opened in the software, the image background was subtracted using a suitable value (to clearly present and distinguish the to-be-targeted particles), and the random noise was removed by filter such as Gaussian blur. A colour threshold was adjusted to make almost every to-be-targeted particle identifiable. The image was made binary, followed by filling hole and watershed, and lastly the implementation of the particle analysis function. The outlines of each particle can be extracted, and the particle size of Feret diameter can be statistically analysed with help from Origin software (2023).

Results and discussion

MALDI-MS to identify main components in bioplastics

First, we employ MALDI-MS to test the bioplastics bags before fragmentation, to analyse the initial components [21]. The results are shown in Fig. 1, where two bioplastic table-bin bags are tested for comparison and to increase the representativeness. Basically, the periodic distribution of the mass spectrum is related with the polymer's periodic chain structure.

Figure 1a is zoomed in as Fig. 1b, where the m/z differences (~ 176) among the main peaks are indicated and can be assigned to the fragments originating from the polymer chain of polybutylene adipate terephthalate (PBAT) or PET presented in (d). That is, MALDI randomly ionises the polymer chain, and generates ions for the subsequent MS analysis. The long chain of the polymer can be broken down by MALDI's laser to oligomers at different chain positions in a random manner, to produce the different length of short chains. Due to the periodic monomer unit in the polymer, the molecular weights of those produced oligomers exhibit a main periodic difference ($\Delta m/z$) of ~ 176 (or ~ 192 , to be discussed below), which originates from monomer or fragment circled in (d). In Fig. 1b, similarly, another periodic m/z difference among the main peaks of ~ 162 can be linked to the monomer in the starch polymer chain, as indicated in (d) too. It can also be linked with the PBAT fragment (m/z of ~ 176) but with a less $-\text{CH}_2$ moiety (m/z of ~ 14).

In the meantime, once further zoomed in as Fig. 1c, a third m/z difference of ~ 18 – 20 is observed, which can be assigned to water molecular (or a similar fragment of H_3O^+) released from the starch, once ionised by the MALDI's laser, as circled in (d) too. Another possibility is that the PBAT fragment or oligomers might lose an oxygen atom during the ionisation process (note the slight difference between the circled parts in Fig. 1d, PBAT fragment has a less oxygen atom than PET monomer), which yields a m/z difference of ~ 18 too if combined with hydrogens. The co-polymer chains of adipate ($\text{C}_6\text{H}_8\text{O}_4$, m/z of ~ 144) and butylene (C_4H_8 , m/z of ~ 56) might be shielded or too weak to be monitored.

To increase the representativeness, we test another kitchen table-bin bag sample, the similar results are collected and presented in Fig. 1e, f. In Fig. 1e, the periodic mass spectrum is observed again, indicating the possible polymer structures. Once zoomed in as (f), the main peak position differences are indicated and marked, with $\Delta m/z$ differences of ~ 176 , ~ 162 and ~ 18 again. There can be associated with the polymer monomer or fragment, the starch monomer and the potential water of the released items. Note the polymers of PBAT and PET have the similar molecular structures, particularly the similar fragments in the polymer chains, as circled in Fig. 1d, leading to their distinguishing difficulty by MALDI-MS [25]. More research is needed here.

Above MALDI-MS results can suggest the main possible components in these bioplastics are polymer and

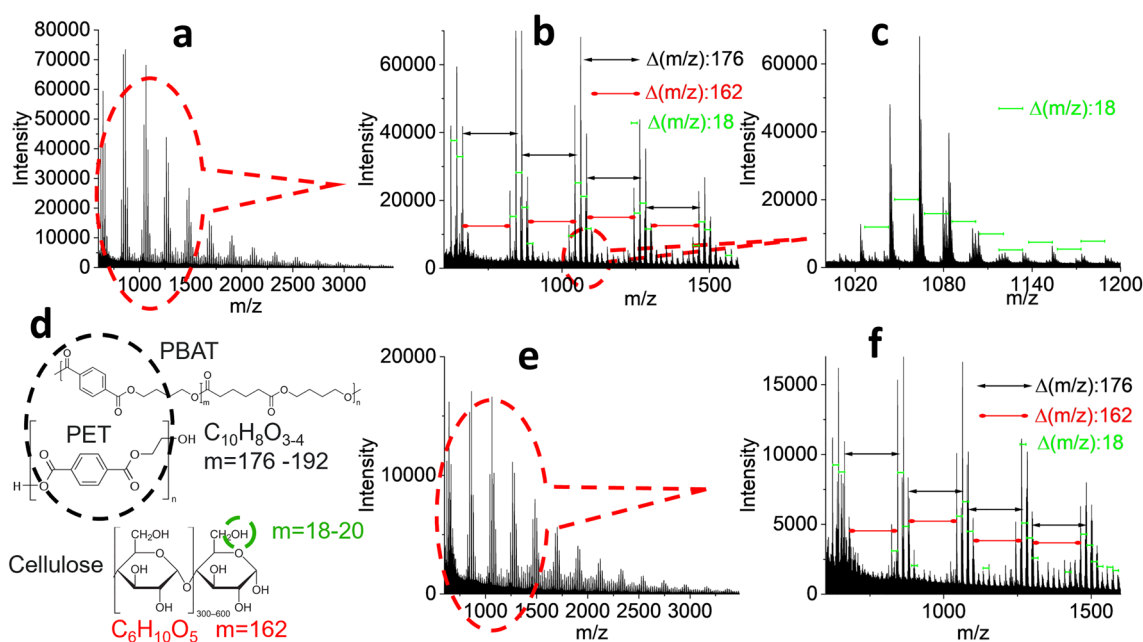


Fig. 1 MALDI-MS results of two samples (a–c, e–f, respectively) before fragmentation, by zooming in the circled parts of the mass spectra. d Suggests the molecular structures of polymers and starch, with the marked monomers or fragments' molecular weights

starch. The exact and detailed formulation is beyond the scope of this report. However, once fragmented such as in kitchen, small debris can be released as bioplastic fragments or microplastics, which is tested below using Raman from molecular spectrum perspective.

Raman imaging to visualise fragmentation

We also test the bioplastics' stability in oven ($\sim 60\text{ }^{\circ}\text{C}$) and in water, the results are presented in Figures S3-S5 (Supporting Information). Basically, the bioplastics is stable for half a year and there is no morphological change in the absence of microorganisms. Some changes happened for the Raman spectra after half a year, suggesting a slow fragmentation process. On the contrary, in the presence of microorganisms, the fragmentation process can happen quickly to release debris, such as ~ 1 week in a kitchen bin as presented in Figures S6-S7 (Supporting Information) and characterised below. The typical SEM images of the released debris are shown Figure S8 (Supporting Information).

Derivate surface groups and microplastic by fragmentation

After ~ 1 week service as the table-bin bag in a kitchen, lots of debris are released in the presence of the food residues. Typical debris is tested and shown in Fig. 2. The fragmentation leads to the modification on the surface group, as evidenced by the spectrum change presented in

Fig. 2b, including the broad background and new peaks (such as at $\sim 685\text{ cm}^{-1}$). For comparison, the standard spectra of PBAT, PET and the "Mother" spectrum collected from the bag before the fragmentation are also presented. The similarity among them can lead to the assignment of the polymer in the compostable plastic to PBAT mainly.

After fragmentation, while the broad background can be assigned to the fluorescence originating from the fragmentation, the newly appeared peak can be mapped as image in Fig. 2d to directly visualise the distribution on the sample surface, along with the characteristic peak of PBAT (e) to visualise the PBAT plastic [22]. Another peak at $\sim 2910\text{ cm}^{-1}$ originates from C-H can be mapped as Fig. 2f to visualise the "organics" [26, 27]. In (a), the Raman image mapping the peak at $\sim 685\text{ cm}^{-1}$ (d) is overlapped onto the photo image, to directly visualise the distribution of the derivate surface group. The well match can suggest the surface modification of the bioplastic and the released microplastic due to the fragmentation. In the meantime, the similar molecular structures and spectra of PBAT and PET cannot be effectively distinguished herein by Raman too [25, 28]. Particularly after the fragmentation, the spectrum gets more complicated, as shown here. In the following parts, we will call them as polymer, no matter they are conventional microplastic (PET) or bioplastic fragment (PBAT), and

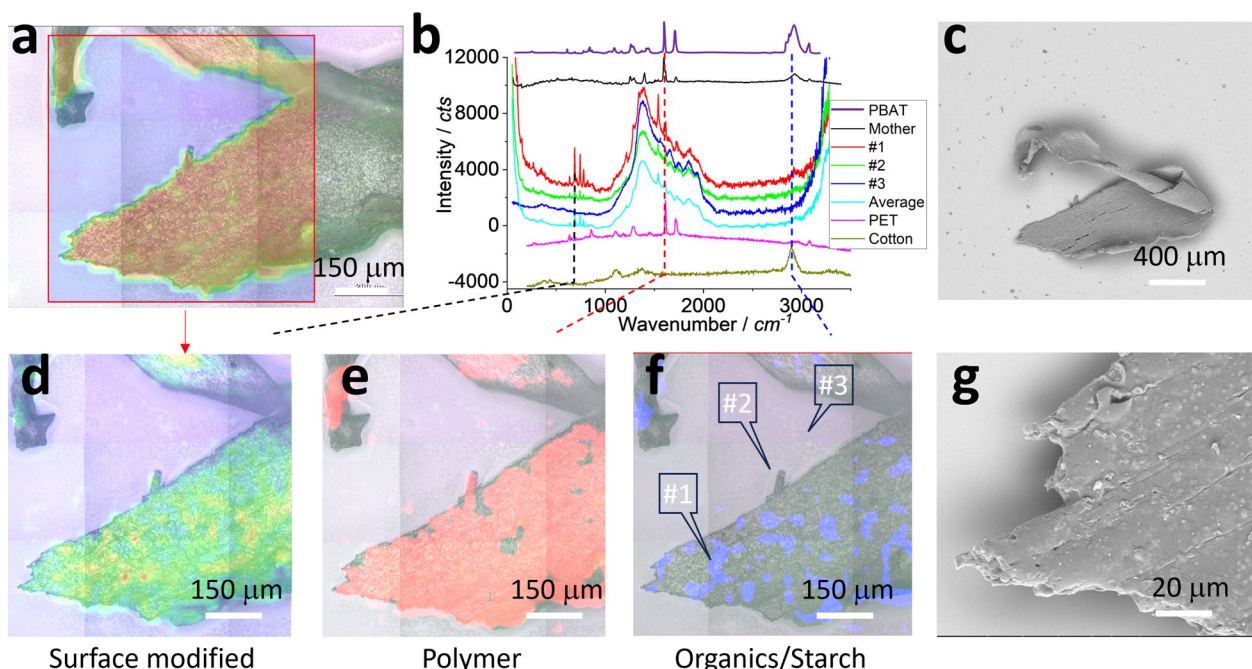


Fig. 2 Photo image (a), Raman spectra (b) / images (d–f) and SEM images (c, g). The compostable bag was biodegraded in a kitchen table-bin for ~ 1 week in the presence of food residues. The spectrum collection positions (#1–3) for (b) are marked in (f). The average spectrum of the scanning matrix is also shown to compare with several reference spectra.

only the spectra of PBAT and “Mother” are presented as reference.

The typical spectra we collected from different positions (marked in Fig. 2f) are presented in Fig. 2b, including a relatively strong one (#1), a middle one (#2) and a blank one (#3) from the non-plastic area that can serve as the background spectrum. During the scanning process, we collected 900 spectra (30×30) as an array of hyper spectrum or a hyperspectral matrix. Their average is also shown in (b). While the spectrum baseline variation has been significantly shrunk, the characteristic peaks are still identifiable, suggesting an increased signal-to-noise ratio. This is the main advantage of Raman imaging analysis via a hyper spectrum [29, 30].

The disadvantage is the mapping is still dependent on the signal of Raman or the signal-to-noise ratio. The signal intensity is controlled by many factors, but the Raman activity of the intrinsic material and the amount of the materials in the target are the key ones. In our case, the bioplastic is mainly formulated with polymer and starch. However, the Raman activity of starch is much weaker than that of polymer and their formulation amount or ratio is not clear. Consequently, although the formulated starch's spectrum can be identified and shown in Figure S9 (Supporting Information), it is usually shielded by the polymer's spectrum. In Fig. 2b, if taking the spectrum of cotton to model that of starch (exact spectrum varies and depends on plant source, purity, etc., but the main monomers of cotton and starch are the same), the mapped image (f) can potentially visualise starch. However, the assignment certainty is low so that we prefer to assign it as “organics”.

The SEM images in Fig. 2c, g show more details about the morphology. The cracks on the plastic debris can be observed in (g), although not visualised via the Raman images. The Raman image's resolution controlled by the scanning pixel size (and the diffraction of the scanning laser) is much lower than that of SEM (such as μm vs. nm). Even so, the Raman image resolution can be improved by shrinking the scanning pixel size, as discussed below.

Zoom in

To get a high resolution of Raman image about the fragmentation debris, we shrink the laser scanning pixel size from $30 \mu\text{m} \times 30 \mu\text{m}$ in Fig. 2 to $2 \mu\text{m} \times 2 \mu\text{m}$ in Fig. 3. In Fig. 3a, the typical Raman spectra are presented. Similar with above, some new peaks appeared (the circled part will be discussed below in Fig. 4), along with the main characteristic peaks of polymer. Similar with above too, the surface modification can be visualised in Fig. 3e, f, by mapping the newly appeared peaks (such as at $\sim 685 \text{ cm}^{-1}$ and $\sim 1536 \text{ cm}^{-1}$). More analysis is provided in Figures S9-S10 (Supporting Information). The characteristic peak of polymer is mapped as image (g), while the organics is mapped as (h). Their patterns are similar in (e–h), again suggesting the derivation of surface group and the released microplastic.

To better present their distributions, we overlap the images in Fig. 3e–h as ones in Fig. 3b, c, to directly compare them. In (b), we merge three images (f, g, h) as one to directly compare their contributions. A good match is observed, suggesting all of them originate from the released debris. To more clearly present them, we merge

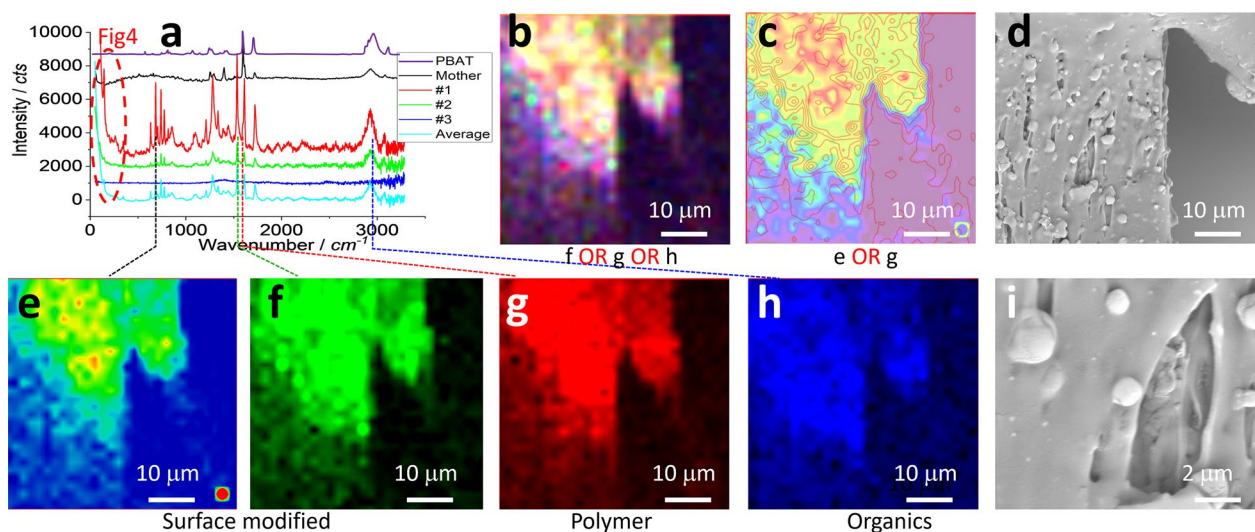


Fig. 3 Zooming-in analysis, including Raman spectra (a), images (b, c, e–h) and SEM images (d, i). b, c) merge (e–h), as suggested on the bottom. In c, only the main contour lines for g are presented. The circled part in a is further analysed in Fig. 4

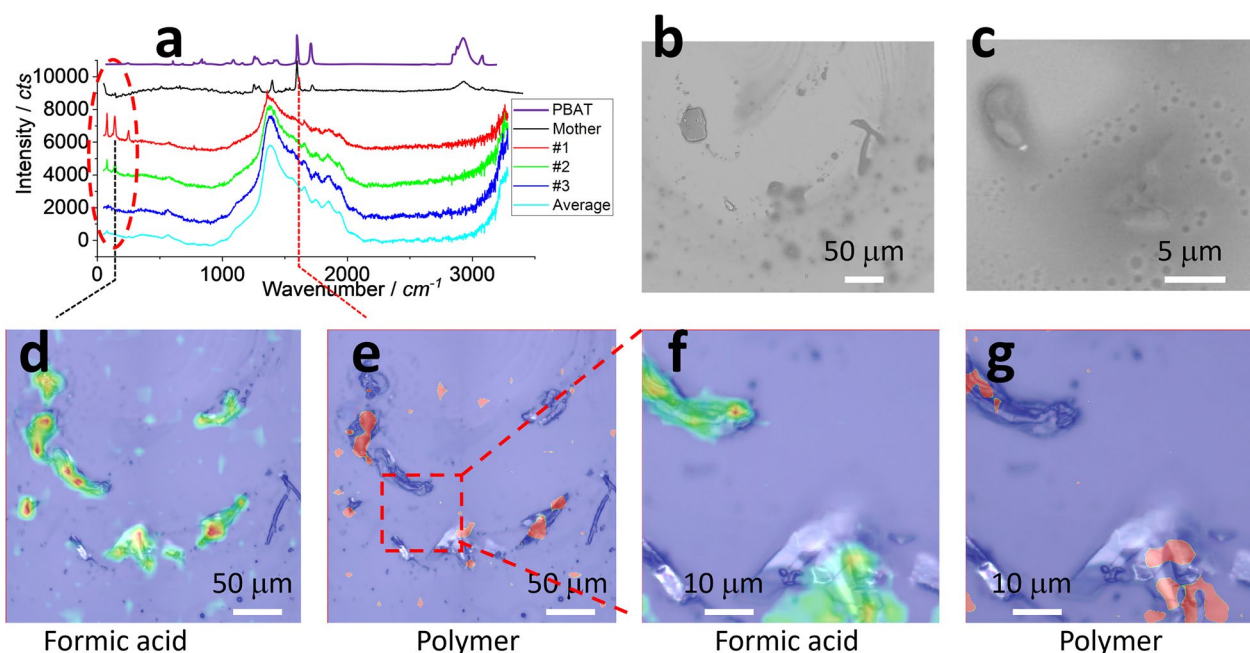


Fig. 4 Released formic acid, including Raman spectrum (a), SEM images (b, c) and Raman images (d–g). The sample was prepared by peeling off a big broken bioplastic debris to expose the left-over on the glass surface. **f, g** Zoom-in of the area squared in **e**

images (e, g) as (c), using the contour lines for image (g) to mark the main distribution of polymer in (c), and compare with the derivate surface group. Again, the match is good, except some parts, which might be due to the different degree of fragmentation at different position.

The SEM images in Fig. 3d, i can provide more details about the morphology. The match between images (c, d, with slight position shift) gets better than that in Fig. 2, due to the shrink in the pixel size of Raman imaging. There might be morphology change after the Raman test and before the SEM test, or occurred during the SEM scanning process due to the electron-beam charging. Anyway, again, the SEM image can provide more details about the tiny structure, particularly in (i). Numerous of dots/spheres are observed on the surface, which is either due to starch or the fragmentation in the presence of bacteria, biota or microorganisms, etc. More research is needed here. In brief, while SEM can provide the morphology information with a high imaging resolution, the chemical information is absent. On the contrary, Raman image can provide the chemical information from the molecular spectrum perspective. Their combination thus can benefit each other, as demonstrated here.

Released formic acid and microplastics by fragmentation

Although we can confirm the surface modification via newly appeared groups derivate on the surface, the identification of their individual molecular structures is difficult, as shown in Figure S10 (Supporting

Information). In the meantime, the fragmentation process is dependent on lots of factors including the microorganism families available in the food residue in the kitchen table. Different microorganisms groups/families can be developed, leading to the different biodegradation process, which further complicates the identification on the biodegradation intermediates [1–5].

To this end, we peeled of the big debris (a film debris) deposited onto the glass surface that have been tested above, to characterise the small pieces left-over on the bottom, as demonstrated in Figure S7 (Supporting Information). The results are shown in Fig. 4. Formic acid is released by the fragmentation and detected. Its characteristic peaks at $\sim 78 \text{ cm}^{-1}$, $\sim 140 \text{ cm}^{-1}$ and $\sim 250 \text{ cm}^{-1}$ are circled in Figs. 3a, 4a [31, 32]. Some of those peaks might be related with the molecular orientation (such as deprotonation) and the detailed assignment is provided in Figure S10 (Supporting Information). One typical peak is mapped as image (d), while the polymer is mapped as (e). The mapped Raman images well match with photo image that works as the image background. Image (d) looks much stronger/brighter than (e). One possible reason is that the intensity of formic acid is stronger than that of polymer, due to their different Raman activities. Another possible reason is that the formic acid covers the polymer microplastic surface and shields the polymer's Raman signal. The third possible reason is that the peak of

polymer is interfered strongly by the spectrum background, such as the broad peak of fluorescence that has been discussed above.

On zooming in the squared area in Fig. 4e, images (f, g) are mapped to visualise formic acid and polymer, respectively. The patterns match well with the background photo image again, suggesting the success of the Raman imaging in capturing the released microplastics and the biodegradation intermediate or product. The slight position shift is due to the different imaging approach. That is, the photo image (serves as the background) is collected via digital camera under the photo illumination, while Raman image is generated by mapping (control by sample stage) the Raman signal (some strong, some weak) excited by laser, collected via a CCD detector [12, 13]. The wavelength is different, the detector/signal is different and the x - y -axis is different. The position mismatch needs a good calibration, particularly for a high magnification of image.

The SEM images in Fig. 4b, c are collected at the approximate same position by aligning the sample under the Raman microscope and the SEM. As said, after the Raman test and before the SEM test, the sample preparation between might change the sample morphology too, such as during the glass-cutting and sputter-coating processes. Some particles might be missed, so that the SEM

image can serve as a reference only, rather than to completely match the Raman image. Once zoomed in, image (c) shows more details, even at nano-scale. These details at nano-scale cannot be effectively mapped by the Raman imaging, due to the resolution issue and weak signal. How to map the nanoplastics using Raman needs more research [18].

Released microplastics by fragmentation

In Fig. 4, although the sample debris was washed and the debris film was deposited onto the glass surface, the sample film might have shielded some items on the bottom. Once the big debris film was peeled off, the shielded ones were exposed so that formic acid has been captured and mapped. In this section, we intentionally washed off the formic acid and other potential biodegradation products/intermediates by prolonging the washing/incubation time from ~ 10 min to ~ 3 days. After that, we conduct an on-site extraction, as shown in Fig. 5a. That is, once a debris is deposited on the glass surface, we add ethanol droplet to cover the sample of the collected debris. Due to the capillary force formed during the evaporation process, “coffee ring” can be formed with some small ones surrounding the central one [20].

The SEM image is collected at the approximated position again, as discussed above. Two squared areas in

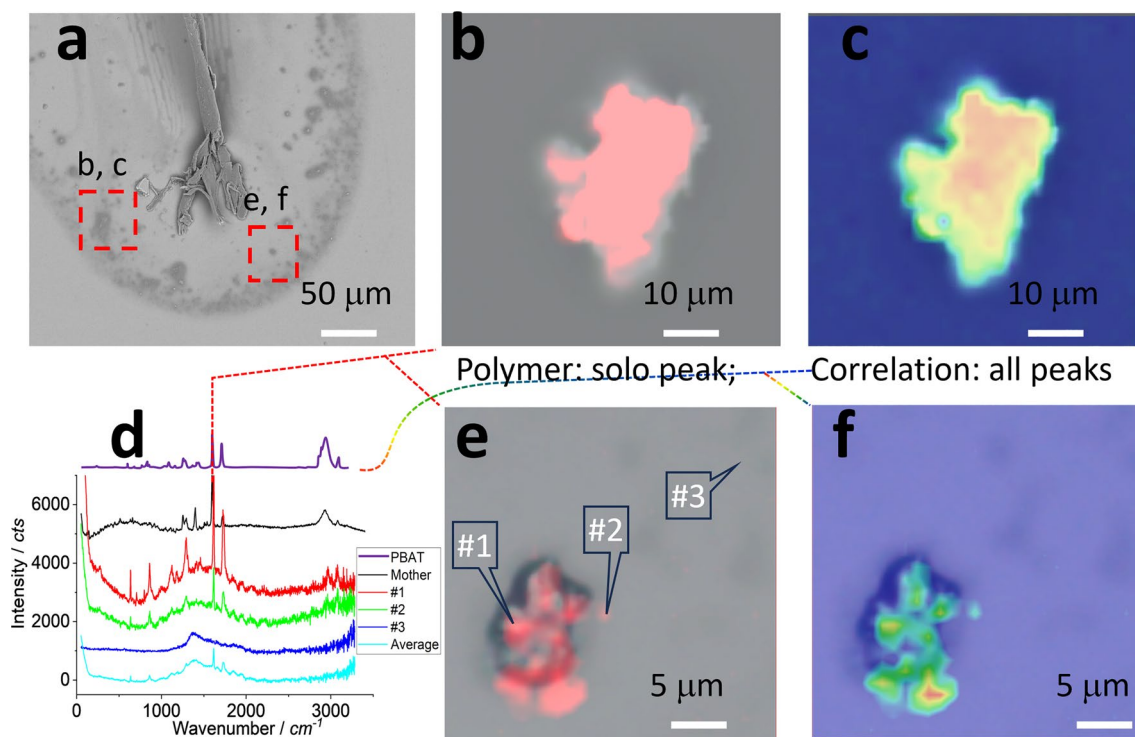


Fig. 5 Released microplastics, including SEM images (a, b, e), Raman images (b, c, e, f) and spectra (d). The sample was prepared by dipping the debris in ethanol for ~ 3 days. Then the debris was deposited on the glass surface and subject to on-site extraction

Fig. 5a are scanned and imaged as (b, c) and (e, f), respectively. Similar with above, the typical spectra are shown in (d), they are well matched with that of PBAT, almost without the co-called “newly appeared” peak observed above (assigned to formic acid). That is, after the biodegradation, washing and on-site extraction, the relatively clean microplastics are captured due to the fragmentation occurring in the table bin within ~1 week. In other words, polymer fragments cannot be effectively and quickly biodegraded, but remain relatively stable against microbial degradation in the observed incubation period of ~1 week, before being collected via bin by the local council. As a main component in the compostable plastic, polymer in the fragment can be persistent to the biodegradation process for a short term (at least ~1 week), cannot be quickly degraded. In general, the release process of microplastics is quick from the bioplastic, when compared to the conventional plastics (e.g. virgin or pure PET) that needs long period of time in nature to fragment as small pieces [25]. However, the long-term persistence of bioplastic fragments is unclear and needs more research.

The images in Fig. 5b, e are generated by mapping the solo peak at $\sim 1620\text{ cm}^{-1}$. The scattering Raman signal is collected as a spectrum in the range of $50\text{--}3300\text{ cm}^{-1}$. Within this range, polymer has many characteristic peaks, as evidenced in (d). A solo peak's image thus means a relatively low signal-to-noise ratio, because other signal beyond this solo peak is missed. The solo peak can also be easily interfered, such as by the background, cosmic ray, signal variation etc. To pick up more signal and to increase the signal-to-noise ratio, the whole set of spectrum should be mapped as a sum to visualise the polymer plastics more accurately [12, 13].

To this end, chemometrics should be involved to effectively decode and interpret the hyper spectrum or the hyperspectral matrix. There are many options, but a simple way is to compare the sample spectrum with the standard spectrum by chemometrics. The comparison and the similarity between them (sample spectrum and standard spectrum) can be easily justified by correlation, which is also commonly used to index a sample spectrum from a database or a spectrum library [23]. The correlation value can be mapped at each pixel and together to generate an image. In this case, the whole set of spectrum, rather than just a solo peak, will take part in the imaging process, meaning an enhanced signal-to-noise ratio, from statistics point of view.

Figure 5c, f are the correlation mapping images. They basically match well with (b, e), respectively. However, the assignment certainty to PBAT microplastics has been enhanced, because the whole set of spectrum is mapped chemometrically. These Raman images can confirm the

release of microplastics or bioplastic fragments. To be general, most of the particles in Fig. 5a can be assigned to the microplastics, and even nanoplastics depending on the size.

Release amount of microplastics or bioplastic fragments

In this section, we count the released debris amount. As said, while the sampling to collect microplastics is difficult and the protocol has not been established [14], we can do on-site extraction, as shown in Fig. 6a, b, using the capillary force formed during the evaporation process [20]. The expansion/shrink of the debris can lead the big debris to move and change the position. Consequently, some small pieces are left behind, on the bottom part in Fig. 6a.

We zoom in and get image in Fig. 6b, which is subjected to particle analysis. To this end, the colour threshold is adjusted, in a hope to “paint” all to-be-analysed particles as red in (c). After being made binary, filling holes and subject to particle analysis, the outlines of the analysed particles can be coloured in (d). The statistical analysis on the size distribution is presented in (e).

Similarly, the sample in Fig. 5a can be converted to Fig. 6f, once the “big debris” is removed. The position shift should be noted, although we tried to conduct the test at the approximately same position, as discussed above. Once subjected to particle analysis, image (g) marks the particles and (h) lists the results. The small ones cannot be assigned to plastic with certainty due to the image resolution issue of Raman, which is also discussed above.

Summarising the results in Fig. 6e, h, we can see that there might be $1100\text{--}2200$ particles/ mm^2 in the size range $1\text{--}25\text{ }\mu\text{m}$. From above tests, most of them can be assigned to microplastics of PBAT. Given that they are quickly released from a kitchen table-bin bag within ~1 week, this aspect could potentially lead to microplastic contamination, such as in the event of littering. Currently there are several open questions including (i) if or not there is any difference between the bioplastic fragments and the conventional microplastics; (ii) how about the persistence, fate, pathway and risk of bioplastic fragments, in short and long terms, all of which need more research.

This estimate has variations. As discussed above, the fragmentation process of bioplastic depends on lots of factors. Different bacteria, bin, food residue, weather / season / temperature, environment might lead to the variations. This release amount can also vary at the different stage of the biodegradation / composting process. The above on-site extraction process can give us a rough amount only and the big ones ($> 25\text{ }\mu\text{m}$) are not effectively counted. Perhaps these big ones can be further degraded

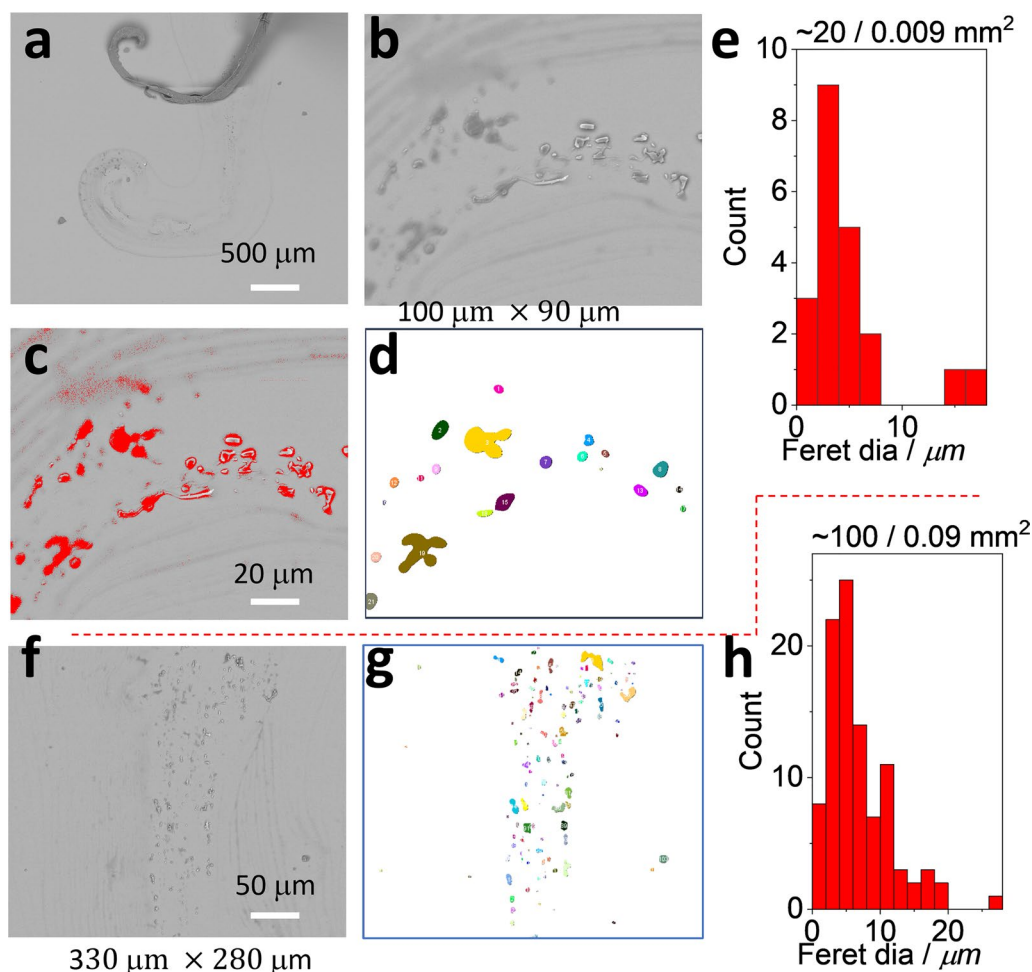


Fig. 6 Particle analysis, including SEM images (**a**, **b**, **f**), colour threshold adjusting image (**c**), particle outlines (**d**, **g**) and statistical results (**e**, **h**). **a** Shows the peeling off a big microplastic lifting behind small ones that are zoomed in as **b**. **b** Is adjusted via colour threshold as **c** to mark the to-be-analysed particles. **d** Lists the outlines of the analysed particles. Their statistical results are presented in **e**. Similarly, **f** is marked as **g** to generate the results in **h**

to release the small ones, for which more research is needed again.

Conclusions

The tested compostable plastic is stable in oven and tap water even for half a year. However, with the involvement of microorganisms, the compostable plastic bag can be easily degraded, to release significant amount of microplastics or bioplastic fragments (in size range of 1–25 μm) within a week. This might be a big concern from the emerging contamination perspective, particularly in the event of littering, i.e. when the bag escapes from waste management and ends up uncontrollably in the environment. Whether or not there is any toxicity difference between the bioplastics-released microplastics and the conventional microplastics is an open question, which should be addressed by further research. The long-term stability or fate of the

bioplastics-released microplastics (such as longer than a week) is also not clear yet. More research is needed to comprehensively understand the fate, transport and potential risk assessment of bioplastics and fragments.

Characterisation of microplastics is still a challenge, which also hampers the risk assessment of bioplastics. With a suitable sample preparation such as on-site extraction and the help from chemometrics, Raman imaging can directly visualise the different surface group and the biodegradation intermediates / products, to monitor the biodegradation process, and to capture microplastics towards quantification. The combination of Raman image with SEM can benefit each other, to identify the components chemically and provide the morphology information at a high resolution, respectively. Further research on microplastics and bioplastics can help to mitigate the plastic pollution gradually and effectively.

Declarations of generative AI and AI-assisted technologies in the writing process

During the preparation of this work the author(s) used ChatGPT in order to write the introduction part. After using this tool/service, the author(s) reviewed and edited the content as needed and take(s) full responsibility for the content of the publication.

Supplementary Information

The online version contains supplementary material available at <https://doi.org/10.1186/s12302-024-00946-1>.

Additional file 1.

Acknowledgements

The authors appreciate the funding support from CRC CARE and the University of Newcastle, Australia. For the Raman measurements and SEM, we also acknowledge the use and support of the South Australian node of Microscopy Australia (formerly known as AMMRF) at Flinders University, South Australia.

Author contributions

C. F. and Z. Z. wrote the main manuscript text and collected the data. All authors reviewed the manuscript.

Data availability

Not applicable.

Declarations

Competing interests

The authors declare no competing interests.

Author details

¹Global Centre for Environmental Remediation (GCER), School of Environmental and Life Sciences, University of Newcastle, Callaghan, NSW 2308, Australia.

²CRC for Contamination Assessment and Remediation of the Environment (CRC CARE), University of Newcastle, Callaghan, NSW 2308, Australia. ³Key Lab of Urban Environment and Health, Institute of Urban Environment, Chinese Academy of Sciences, Xiamen 361021, China.

Received: 7 February 2024 Accepted: 16 June 2024

Published online: 24 June 2024

References

- Rosenboom J-G, Langer R, Traverso G (2022) Bioplastics for a circular economy. *Nat Rev Mater* 7(2):117–137
- Özdamar EG, Ateş M (2018) Rethinking sustainability: a research on starch based bioplastic. *J Sustain Constr Mater Technol* 3(3):249–260
- Agustin MB et al (2014) Bioplastic based on starch and cellulose nanocrystals from rice straw. *J Reinf Plast Compos* 33(24):2205–2213
- Shruti VC, Kutralam-Muniasamy G (2019) Bioplastics: missing link in the era of microplastics. *Sci Total Environ* 697:134139
- Fojt J et al (2020) A critical review of the overlooked challenge of determining micro-bioplastics in soil. *Sci Total Environ* 745:140975
- Allemann MN et al (2024) Rapid biodegradation of microplastics generated from bio-based thermoplastic polyurethane. *Sci Rep* 14(1):6036
- Filella M, Turner A (2023) Towards the global plastic treaty: a clue to the complexity of plastics in practice. *Environ Sci Eur* 35(1):99
- Mohamed Nor NH et al (2021) Lifetime accumulation of microplastic in children and adults. *Environ Sci Technol* 55(8):5084–5096
- Silva AB et al (2018) Microplastics in the environment: challenges in analytical chemistry—a review. *Anal Chim Acta* 1017:1–19
- Hartmann NB et al (2019) Are we speaking the same language? Recommendations for a definition and categorization framework for plastic debris. *Environ Sci Technol* 53(3):1039–1047
- Mitrano DM, Wohlleben W (2020) Microplastic regulation should be more precise to incentivize both innovation and environmental safety. *Nat Commun* 11(1):5324
- Fang C, Luo Y, Naidu R (2023) Microplastics and nanoplastics analysis: options, imaging, advancements and challenges. *TrAC, Trends Anal Chem* 166:117158
- Fang C, Luo Y, Naidu R (2023) Advancements in Raman imaging for nanoplastic analysis: challenges, algorithms and future perspectives. *Anal Chim Acta* 1290:342069
- Ivleva NP (2021) Chemical analysis of microplastics and nanoplastics: challenges, advanced methods, and perspectives. *Chem Rev* 121(19):11886–11936
- Kooi M et al (2021) Characterizing the multidimensionality of microplastics across environmental compartments. *Water Res* 202:117429
- Rocha-Santos T, Duarte AC (2015) A critical overview of the analytical approaches to the occurrence, the fate and the behavior of microplastics in the environment. *TrAC, Trends Anal Chem* 65:47–53
- Wille G, Schmidt U, Hollricher O (2018) RISE: correlative confocal Raman and scanning electron microscopy. *Confocal Raman Microscopy*, p. 559–580
- Fang C, Luo Y, Naidu R (2023) Super-resolution imaging of micro- and nanoplastics using confocal Raman with Gaussian surface fitting and deconvolution. *Talanta* 265:124886
- Fang C, Luo Y, Naidu R (2023) Super-resolution Raman imaging towards visualisation of nanoplastics. *Anal Methods* 15(40):5300–5310
- Wong T-S et al (2011) Nanochromatography driven by the coffee ring effect. *Anal Chem* 83(6):1871–1873
- Luo Y et al (2022) Raman imaging and MALDI-MS towards identification of microplastics generated when using stationary markers. *J Hazard Mater* 424:127478
- Sobhani Z et al (2019) Identification and visualisation of microplastics by Raman mapping. *Anal Chim Acta* 1077:191–199
- Luo Y et al (2022) Dual-principal component analysis of the Raman spectrum matrix to automatically identify and visualize microplastics and nanoplastics. *Anal Chem* 94(7):3150–3157
- Bescond A et al (2014) Automated determination of aggregate primary particle size distribution by TEM image analysis: application to soot. *Aerosol Sci Technol* 48(8):831–841
- Yang Y et al (2023) Complete bio-degradation of poly(butylene adipate-co-terephthalate) via engineered cutinases. *Nat Commun* 14(1):1645
- Yang Y-H, Wang T (1997) Fourier transform Raman spectroscopic characterization of humic substances. *Vib Spectrosc* 14(1):105–112
- Donelli I et al (2009) Enzymatic surface modification and functionalization of PET: a water contact angle, FTIR, and fluorescence spectroscopy study. *Biotechnol Bioeng* 103(5):845–856
- Cai Y, Lv J, Feng J (2013) Spectral characterization of four kinds of biodegradable plastics: poly (Lactic Acid), Poly (Butylenes Adipate-Co-Terephthalate), Poly (Hydroxybutyrate-Co-Hydroxyvalerate) and Poly (Butylenes Succinate) with FTIR and Raman spectroscopy. *J Polym Environ* 21(1):108–114
- Khan MJ et al (2018) Modern trends in hyperspectral image analysis: a review. *IEEE Access* 6:14118–14129
- Lu B et al (2020) Recent advances of hyperspectral imaging technology and applications in agriculture. *Remote Sens* 12(16):2659
- Olbert-Majkut A et al (2009) Raman spectroscopy of formic acid and its dimers isolated in low temperature argon matrices. *Chem Phys Lett* 468(4):176–183
- Pinkard B et al (2019) Kinetics of formic acid decomposition in subcritical and supercritical water—a Raman spectroscopic study. *Int J Hydrogen Energy* 44(60):31745–31756

Publisher's Note

Springer Nature remains neutral with regard to jurisdictional claims in published maps and institutional affiliations.